

MEDICAL ROBOTS

Metabolically efficient walking assistance using optimized timed forces at the waist

Prokopios Antonellis^{1,2*}, Arash Mohammadzadeh Gonabadi^{1,3}, Sara A. Myers^{1,4}, Iraklis I. Pipinos^{4,5}, Philippe Malcolm^{1*}

Copyright © 2022
The Authors, some
rights reserved;
exclusive licensee
American Association
for the Advancement
of Science. No claim
to original U.S.
Government Works

The metabolic rate of walking can be reduced by applying a constant forward force at the center of mass. It has been shown that the metabolically optimal constant force magnitude minimizes propulsion ground reaction force at the expense of increased braking. This led to the hypothesis that selectively assisting propulsion could lead to greater benefits. We used a robotic waist tether to evaluate the effects of forward forces with different timings and magnitudes. Here, we show that it is possible to reduce the metabolic rate of healthy participants by 48% with a greater efficiency ratio of metabolic cost reduction per unit of net aiding work compared with other assistive robots. This result was obtained using a sinusoidal force profile with peak timing during the middle of the double support. The same timing could also reduce the metabolic rate in patients with peripheral artery disease. A model explains that the optimal force profile accelerates the center of mass into the inverted pendulum movement during single support. Contrary to the hypothesis, the optimal force timing did not entirely coincide with propulsion. Within the field of wearable robotics, there is a trend to use devices to mimic biological torque or force profiles. Such bioinspired actuation can have relevant benefits; however, our results demonstrate that this is not necessarily optimal for reducing metabolic rate.

INTRODUCTION

Robots often incorporate anthropomorphic designs (1). In the sub-field of rehabilitation robotics, different groups develop biologically inspired exoskeletons that assist with moments at the biological joints (2). Although exoskeletons have appropriate applications, simple pendulum models suggest that timed linear forces acting through the center of mass (COM) can actuate walking more efficiently than moments (3). Gottschall and Kram (4) conducted foundational research on the effects of linear forward aiding forces with constant magnitude at the COM and show that the metabolic rate of walking in healthy adults can be reduced by up to 47% with a long elastic tether. They report that optimal aiding forces minimize propulsion at the expense of increased braking ground reaction forces (GRFs) and called for further research on devices that could specifically assist propulsion, perhaps without impeding braking.

There is increasing interest in devices that can apply such non-constant force profiles during specific phases of the gait cycle (5, 6). Bhat *et al.* (5) used stiff tethers to elicit cyclic force profiles from the back-and-forth movements on a treadmill. They found smaller metabolic rate reductions than those for constant forces (4, 7), which suggests that their force profiles are suboptimal. Penke *et al.* (6) used a pulley system that connected the COM to one of the ankles to apply cyclic force profiles. This system reduced the metabolic rate of individuals poststroke by 12%, demonstrating potential clinical applicability. In healthy participants, they found relatively smaller

reductions than those for constant forces, which suggests that there is room for further improvements.

Certain clinical populations have large increases in metabolic rate during walking [e.g., 200 to 300% in cerebral palsy (8)]. Exoskeletons can currently reduce the metabolic rate by up to one-fourth in healthy individuals (9, 10). Even if, potentially, similar reductions in metabolic rate versus unassisted walking could be obtained in clinical populations, this might be insufficient to bring the metabolic cost to normal levels and allow for sustained walking practice in certain patients who have a metabolic cost that is higher compared with healthy individuals. In the current study, we investigate different ways of assisting treadmill walking using timed forward forces at the COM instead of exoskeletons. Simple pendulum models (3) and studies with exoskeletons (9–14) show that the parameters that define the shape of the actuation profile during the walking cycle can influence the metabolic rate. We aimed to investigate the effects of timing and magnitude for nonconstant force profiles at the COM in healthy individuals. This initial work is intended to assess this type of assistive strategy at the COM using a robotic tether system with the goal of reducing the metabolic rate of walking in healthy adults. Depending on the outcome, this could be a preliminary step toward potentially testing such a system in clinical populations. Gottschall and Kram (4) reported that the metabolically optimal magnitude for constant forces minimizes propulsion. Therefore, we expected a similar relationship between propulsion reduction and metabolic rate reduction, and we hypothesized that nonconstant force profiles in which the peak magnitude coincides with propulsion would optimally reduce propulsion and metabolic rate.

RESULTS

Robotic waist tether experiments

We conducted experiments with a cable robot that applied forces to a waist belt in 10 healthy participants (Fig. 1A and movie S1) (15, 16). A force control algorithm was used to apply 32 conditions with

¹Department of Biomechanics and Center for Research in Human Movement Variability, University of Nebraska at Omaha, 6160 University Drive South, Omaha, NE 68182, USA. ²Department of Neurology, School of Medicine, Oregon Health & Science University, 3181 SW Sam Jackson Park Road, OP-32, Portland, OR 97239, USA. ³Rehabilitation Engineering Center, Institute for Rehabilitation Science and Engineering, Madonna Rehabilitation Hospital, 5401 South Street, Lincoln, NE 68506, USA. ⁴Department of Surgery and Research Service, Veterans Affairs Nebraska-Western Iowa Medical Center, Omaha, NE 68105, USA. ⁵Department of Surgery, University of Nebraska Medical Center, 982500 Nebraska Medical Center, Omaha, NE 68198, USA. *Corresponding author. Email: antonelp@ohsu.edu (P.A.); pmalcolm@unomaha.edu (P.M.)

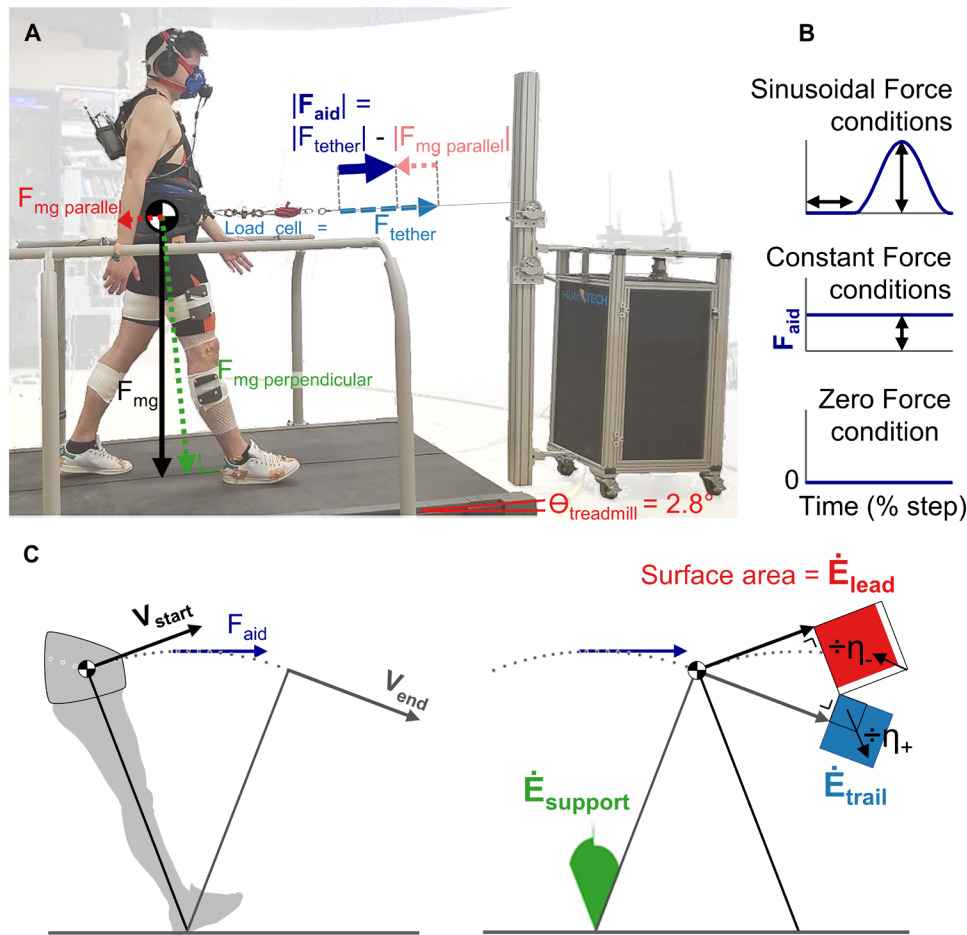


Fig. 1. Experimental conditions and simulation model. (A) Photograph of the robotic waist-tether setup. A cable robot (HuMoTech, Pittsburgh, PA, USA) applied force profiles to a waist belt. To avoid the tether going slack during portions of the step cycle, a constant backward force was simulated by inclining the treadmill (17, 62) by a 2.8° angle. The reported aiding forces are the forces measured with a load cell minus the parallel component of gravity. (B) Schematic of the force profile conditions. We used the cable robot to apply Sinusoidal Force conditions, Constant Force conditions, and a Zero Force condition. (C) Simple pendulum model. We modeled an inverted pendulum (3, 18) with the mean mass and leg length of our participants. This model was used to simulate different aiding force timings and magnitudes. For each condition, we identified the initial COM velocity required to match the experimental step time and the velocity at the end of single support. On the basis of COM velocity, we estimated the metabolic rate (visualized as colored surfaces) of the trailing and leading legs during the step-to-step transition and the support leg during single support (15). The metabolic rate of the step-to-step transition was estimated by dividing the redirection work rate that the legs have to produce (3) by the assumed efficiencies (19).

sinusoidal force profiles with desired magnitudes, timings, and durations (Sinusoidal Force conditions; Fig. 1B) (17) as well as 4 conditions where the force had a constant magnitude throughout the step cycle (Constant Force conditions). Because the tether acts symmetrically on both legs, we could not differentiate between the effects of assisting during phases associated with one specific leg (e.g., first or second double support phase). However, we could differentiate between effects associated with the activities of both legs (e.g., single or double support); hence, we expressed actuation timings in percent of the step cycle instead of percent of the stride cycle. We calculated the net aiding work rate by multiplying the net aiding force by the COM velocity, and we estimated the metabolic rate using respiratory measurements.

Participants attended a habituation session and a testing session during which they walked under 36 different force profiles that were randomized and grouped into three blocks, each separated by 10 min of rest (fig. S12A). The force conditions were combinations of three desired durations, four desired onset timings, and different desired peak net aiding force magnitudes. The experiment was conducted using our robotic waist tether system (17), which was developed based on a commercially available actuation and control platform (HuMoTech, Pittsburgh, PA, USA; Fig. 1A, movie S1, and table S1). We conducted tests with 10 male participants walking on a treadmill at 1.25 m s^{-1} .

Effects of force profiles on metabolic rate

The greatest significant reduction in metabolic rate compared with the condition with a net aiding force of zero (Zero Force condition) was $47.8 \pm 4.7\%$ (mean \pm SEM, $P < 0.001$, paired t test with Holm-Šidák correction; Fig. 2A). This reduction occurred in the Sinusoidal Force condition with a peak force of $15.0 \pm 0.5\%$ body weight (BW), a duration of $64.1 \pm 1.6\%$ of the step, and a peak timing during the double support phase at $21.1 \pm 0.3\%$ of the step. The smallest reduction in metabolic rate was $9.1 \pm 2.0\%$. This reduction was also significant ($P = 0.006$) and occurred in the condition with a peak force of $4.7 \pm 0.1\%$ BW, a duration of $27.0 \pm 0.4\%$, and a peak timing of $50.9 \pm 0.4\%$ of the step.

A mixed-effects model analysis of the effects of the different actuation profile parameters showed a significant effect of peak timing on metabolic rate [$P_{P_{\text{peak-sin}}(\text{peak})} < 0.001$] with an optimum at the middle of the double support phase ($15.1 \pm 0.1\%$ of step time; Fig. 2B).

As expected, different conditions reduced metabolic rate by different amounts, but, unexpectedly, there were no conditions that increased the metabolic rate. Humans appear to be less sensitive to the timing of assistance at the COM than that of joint-level assistance, because certain conditions in studies with exoskeletons increase the metabolic rate (11, 14).

We found a significant U-shaped trend in the effect of net aiding work rate ($P_{W_{\text{aid}}} \text{ and } P_{W_{\text{aid}}^2} < 0.001$) with an optimum at $0.958 \pm 0.043 \text{ W kg}^{-1}$ (Fig. 2C). There was no significant effect of net aiding power duration. The best Sinusoidal Force condition produced a significantly greater reduction in metabolic rate per unit net aiding work rate than the best Constant Force condition (ratios were 2.06 ± 0.21 and 1.54 ± 0.14 , respectively, $P = 0.032$), but there was

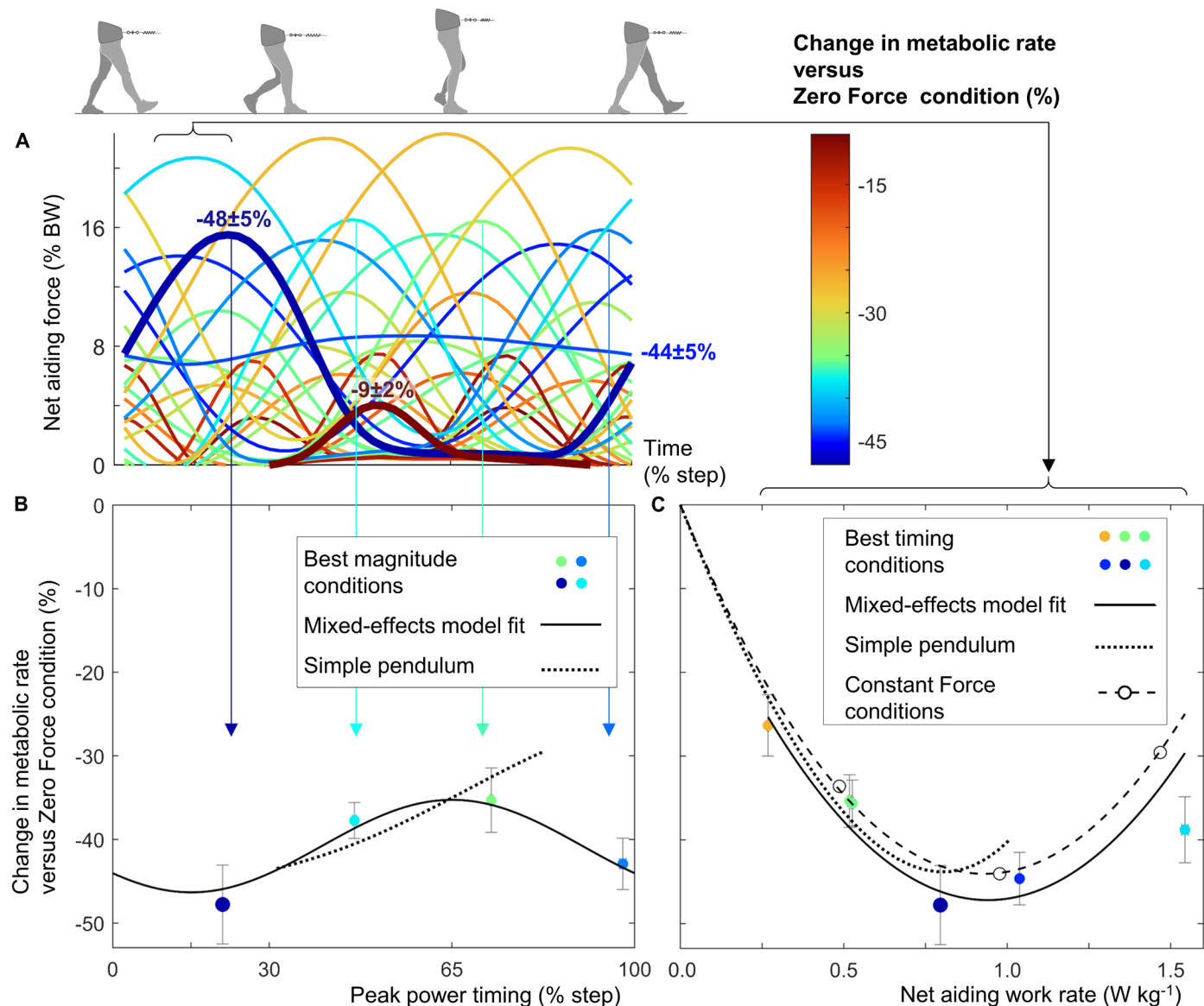


Fig. 2. Effects of force profiles on metabolic rate. (A) Net aiding forces and corresponding metabolic rate reductions. Lines represent the means of the participants for the Sinusoidal Force conditions and the best Constant Force condition. The color scale indicates metabolic rate reduction. Thick lines indicate the highest and lowest reductions. We applied the same profile during left and right steps; therefore, we plotted profiles versus step instead of stride time. **(B)** Effect of peak timing on metabolic rate. Dots and error bars represent means and SEMs of participants for conditions with different timings but approximately the same duration and net aiding work rate as the condition with the highest reduction. Solid line represents the mixed-effects model fitted on all Sinusoidal Force conditions evaluated at the mean magnitude of dots. Dotted line represents the estimation from the simple pendulum simulated over the feasible range. **(C)** Effect of net aiding work rate on metabolic rate. Dots and error bars represent means and SEMs for conditions with different net aiding work rates within a timing range of $\pm 6\%$ from the optimum (15.1%). Circles and the dashed line represent Constant Force conditions. Independent variables of (B) and (C) were selected from different candidate metrics (15). *P* values of reductions in metabolic rate versus Zero Force condition were smaller than 0.05 for all conditions (paired *t* test with Holm-Sidak correction, $n = 10$).

no significant difference in the metabolic rate. We also used the fits of the mixed-effects model analysis equation to each participant to improve the estimates of the individual optima. This analysis suggests that there was still a small but significant metabolic rate benefit of $3.9 \pm 1.5\%$ of the optima of the Sinusoidal Force conditions compared with the optima of the Constant Force conditions ($P = 0.030$). The highest reduction in the metabolic rate of the Constant Force conditions ($44.0 \pm 4.4\%$) and the Constant Force level that minimized the metabolic rate ($7.9 \pm 0.03\%$ BW) were similar to other studies

[47% with a net aiding force of 10% BW (4), 35% with a net aiding force of 8% BW (7), and 34% with a net aiding force of 8.4% BW (6)].

Interpretation using inverted pendulum model

To understand the potential underlying mechanisms of the effects seen during experimentation, we conducted an inverted pendulum simulation (3, 18) and analyzed relevant biomechanical measurements. The simple pendulum model (Fig. 1C) reproduced the changes observed in metabolic rates with increasing net aiding work

rate but reached its optimum at a lower work rate (0.796 W kg^{-1} ; Fig. 2C). The model also closely reproduced the effect of assistance timing over the feasible simulation range. The model could not simulate timings at the beginning of the step because double support is instantaneous. In addition, the model could not simulate timings at the end of the step. This occurred because the centripetal component from gravity minus the component from the tether force that pulls the COM away from the ground contact point (due to the alignment between the tether and the leg) was not sufficient to sustain the radial acceleration (Fig. 2B). We plotted the results from the model over the time range that corresponds to the single support phase from the human experimental data (immediately after toe-off at 30% of

the step cycle until the end of the feasible simulation range). This simple model explained that aiding forces early in the step cycle were optimal because they help accelerate the COM, thereby reducing the positive leg work required to reach the apex of the inverted pendulum movement. Aiding force after midstance was suboptimal because the COM spontaneously accelerates due to gravity.

Effects on GRFs and COM velocity

We found significant effects of net aiding work rate and peak timing on the propulsion part of the bipedal sum of the GRF (all P values < 0.001 , mixed-effects model analysis; Fig. 3A and table S4). As expected, the peak timing that resulted in the greatest propulsion

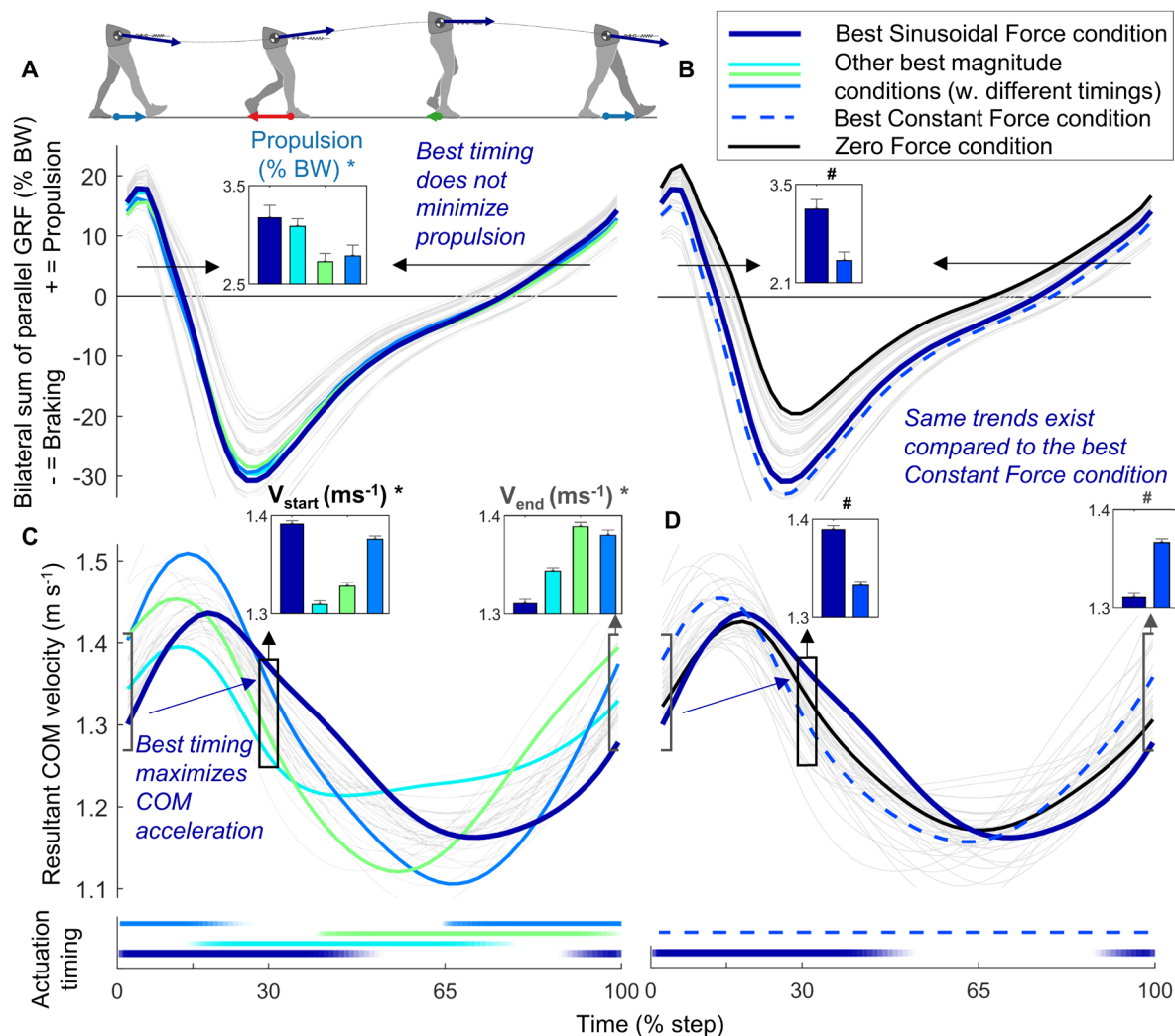


Fig. 3. Effects of timing on GRF and COM velocity. (A) Effect of timing on bilateral parallel GRF. The tether does not act unilaterally on one leg; therefore, we chose to analyze the bilateral GRF instead of the unilateral GRF. Colored lines represent the means of participants from conditions with similar actuation magnitudes and approximately the same net aiding work rate as the best condition from Fig. 2B but with different timings. The GRFs of the colored conditions appear offset because of the net aiding force that is not shown here. Gray lines represent all other conditions. Bar plots represent the average propulsion GRF averaged over the entire step duration. The thick line marks the condition that showed the highest metabolic rate reduction. (B) Comparison of bilateral parallel GRF between the condition with the highest reduction in metabolic rate (thick blue line), best Constant Force condition (dashed blue line), and Zero Force condition (black line). (C) Effect of timing on the resultant COM velocity. Bar plots represent the magnitude of the COM velocity vector at the beginning and end of single support. Horizontal lines represent the actuation periods. The condition with the highest reduction in metabolic rate (dark blue bar) has the lowest COM velocity at the end of single support, the highest COM velocity at the beginning of single support, and thus the highest acceleration during double support. (D) Comparison of COM velocity between the condition with the highest reduction in metabolic rate (thick blue line), best Constant Force condition (dashed blue line), and Zero Force condition (black line). * means P value of effect of peak timing < 0.05 . # means P value of paired t test versus Best Constant Force condition < 0.05 ($n = 10$).

reduction fell inside the propulsion phase (mean \pm SEM of the peak timing that minimized propulsion was $74.7 \pm 0.2\%$ of step, mixed-effects model analysis). However, the influence of timing on propulsion GRF was small (range between minimum and maximum propulsion GRFs of conditions with the same magnitude in Fig. 3A is $0.6 \pm 0.1\%$ BW). Even force profiles that fell entirely during the braking phase also significantly reduced propulsion by up to $36.5 \pm 1.6\%$ at the expense of a significant increase in braking GRF and significantly reduced the metabolic rate by up to $37.7 \pm 2.1\%$ compared with the Zero Force condition ($P < 0.001$, paired t tests with Holm-Šidák correction). Contrary to our hypothesis, the peak timing that minimized metabolic rate based on the mixed-effects model analysis (15.1% of step time) aligned with the transition from propulsion to braking (the first zero crossing occurred at $15.4 \pm 0.6\%$ of step time, mean \pm SEM from all conditions; Fig. 3A) instead of aligning with the middle of the propulsion phase. The simple pendulum model proved to better explain our results than the GRF hypothesis. We found large significant effects of peak timing on the resultant COM velocity at the beginning and end of single support ($P < 0.001$; Fig. 3B and table S4). The metabolically optimal timing

was close to the timing that maximized the COM velocity at the beginning of single support (the peak timing that maximized initial COM velocity was $10.0 \pm 0.6\%$ of step time, mixed-effects model analysis). The peak timings that minimized leading leg negative work and trailing leg positive work all occurred in the first half of single support, as predicted by the model. The peak actuation timings that minimized collision and push-off were 32.6 ± 1.3 and $54.0 \pm 0.5\%$ of step, respectively, and the middle of single support was at 65% (all P values for timing < 0.001 ; table S4). These results confirmed the model prediction that assisting COM acceleration at the beginning of the step reduces the required leg work (Fig. 4). The Sinusoidal Force condition that minimized the metabolic rate significantly increased not only the required propulsion by $15.1 \pm 0.6\%$ compared with the best Constant Force condition ($P < 0.001$; Fig. 3B) but also the COM acceleration compared with the best Constant Force condition. Specifically, the Sinusoidal Force condition had $4.6 \pm 0.2\%$ greater COM velocity at the beginning of the single support and $6.1 \pm 0.2\%$ smaller COM velocity at the end of the single support compared with the best Constant Force condition (all P values < 0.001 ; Fig. 3C). This shows that the Sinusoidal Force

Downloaded from https://www.science.org at The Hong Kong University of Science and Technology (Guangzhou) on May 25, 2026

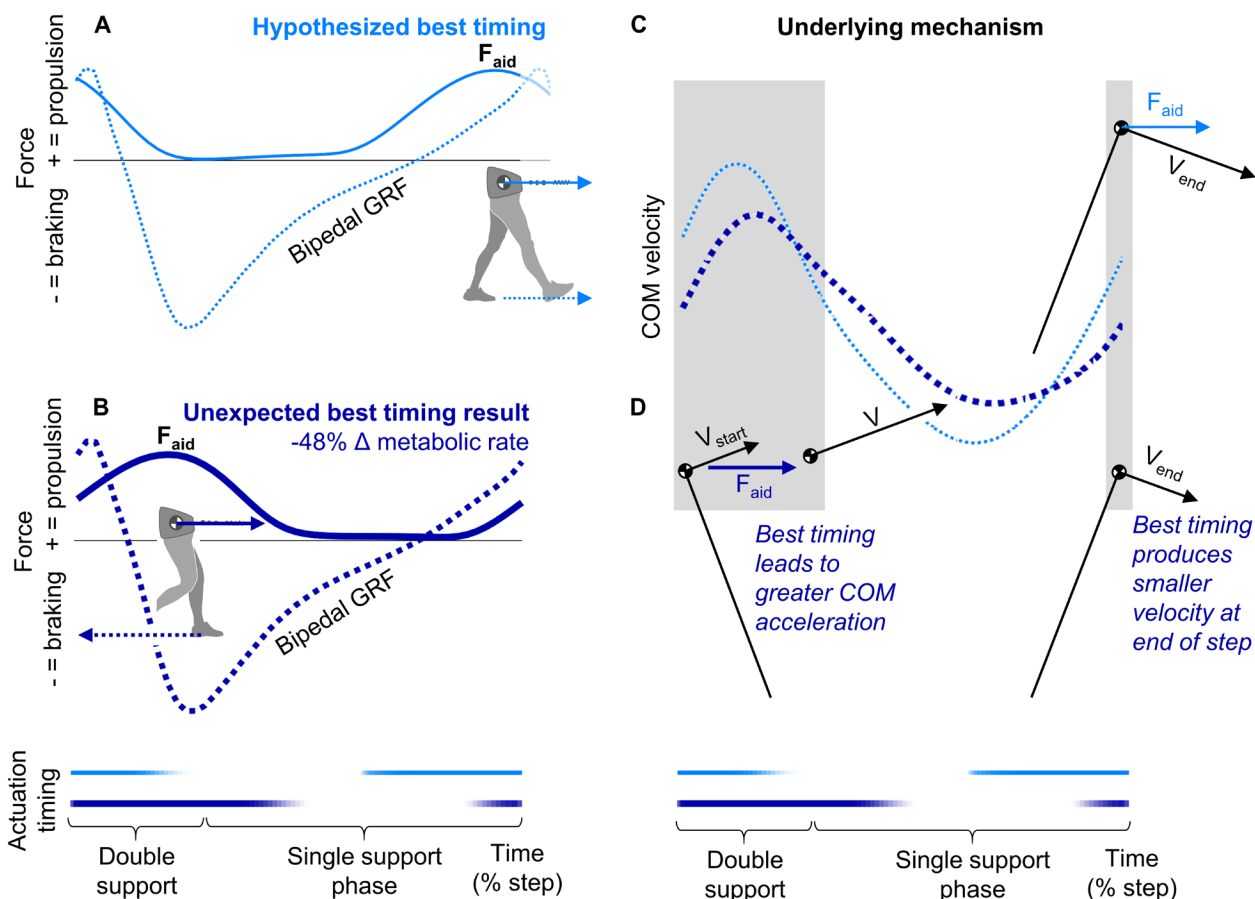


Fig. 4. Hypothesis and underlying mechanism. (A) Hypothesized best timing of a Sinusoidal Force condition. The plot shows the mean net aiding force (solid line) and the bipedal sum of the parallel GRF (dashed line) from the participants in the Sinusoidal Force condition where the net aiding force matches closest to the bipedal propulsion timing, plotted versus step time. (B) Best timing result. Condition with the highest reduction in metabolic rate. (C) Explanation based on COM velocity effect. Plot showing the mean COM velocity of all participants of the conditions with the hypothesized best timing and the highest metabolic rate reduction. (D) Simple pendulum model. Stick figures show the higher COM acceleration at the beginning of the step and lower COM velocity at the end of the step in the condition with early peak timing compared with the condition with late peak timing. The pendulum model predicts that the higher initial acceleration and lower final velocity will result in lower positive and negative leg work rates required to redirect the COM ($n = 10$).

conditions reduce the metabolic rate in a different way than the Constant Force condition, not primarily by reducing propulsion GRF.

Proof-of-concept studies in impaired gait and patients

As an initial evaluation of the applicability of the waist tether in impaired gait, we conducted an experiment in a healthy participant in which we induced a nonconstant COM velocity by unilaterally restricting plantarflexion. The results of this single-participant experiment suggest that it is possible to change the metabolic rate from +2 to -42% compared with the Zero Force condition or +7 to -35% compared with a No Tether condition using different Sinusoidal Force profiles after one habituation session. We also conducted an experiment to evaluate the feasibility of using the waist tether system as a method of exercise therapy in patients with limited mobility due to a prevalent disease. Two patients with symptomatic peripheral artery disease (PAD) walked with the waist tether during two sessions, referred to as habituation and testing sessions. During the testing session, we performed repeated comparisons between a Sinusoidal Force condition with low peak force and peak timing during double support and a No Tether condition, and we found reductions in metabolic rate of 12.0 and 9.7% in one patient and 23.1 and 20.1% in the second patient (15).

Comparison with literature on linear and angular assistance devices

Plotting reductions in metabolic rate versus net aiding work rate allows for comparing results with devices that provide angular assistance, such as exoskeletons (Fig. 5). This analysis confirmed that applying constant aiding forces with tethers (4, 7) has similar effects as downhill walking (19, 20). Nonconstant force profiles obtained

with passive tether systems that were tested in healthy adults have peak timings around 85% of the step time (5, 6), and this was close to the least optimal timing according to our data (65.1%). This result could explain their smaller observed reductions in healthy participants. Reductions in metabolic rate in $W\text{ kg}^{-1}$ from the Sinusoidal Force conditions with the best timing were greater than the best-in-class results for a wide range of devices, including exoskeletons and prostheses (all P values ≤ 0.036 , t tests) (4–7, 9–14, 16, 21, 22), except for one condition in a study (6) that uses constant aiding force in healthy participants ($P = 0.691$, one-sample t test).

DISCUSSION

The field of wearable robotics has evolved from sophisticated full-body exoskeletons (2) toward simpler single-joint exoskeletons that first achieved metabolic rate reduction (9, 21, 22). Our study suggests that a simpler strategy of accelerating the COM with linear forces can provide further gains in stationary applications such as treadmill exercise therapy. Although robotic tethers cannot assist with over-ground mobility similar to exoskeletons, the greater reductions could enable treadmill exercise therapy applications.

Clinical practice guidelines recommend that combining robotic assistance with higher intensity stepping is an area that remains to be investigated (23). The large effects of robotic waist tether assistance could allow for higher intensity stepping training. However, it remains to be seen whether the effects observed in healthy participants transfer to patients. Although the effect of timing on the horizontal GRF was small, we found large effects on the COM velocity. Using their pulley mechanism that allowed for applying nonconstant force profiles, Penke *et al.* (6) found a 12% reduction

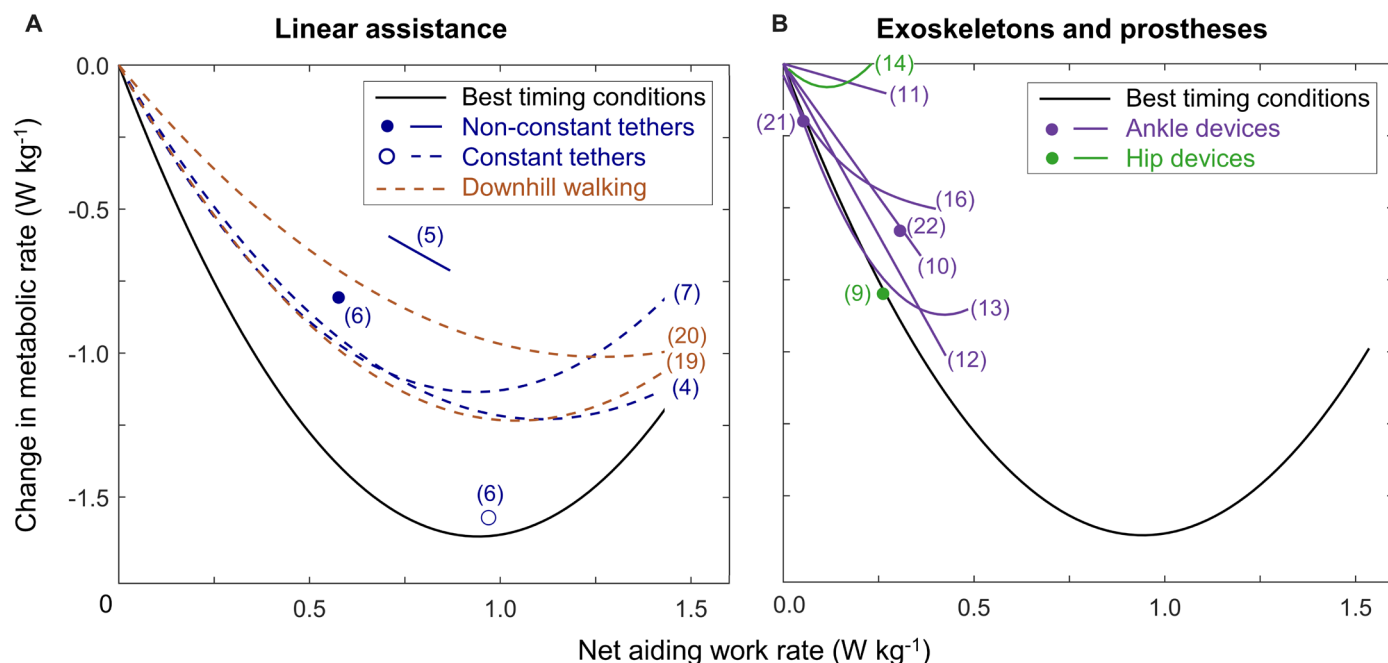


Fig. 5. Literature comparison within the field of wearable robotics. (A) Studies with linear assistance strategies (constant and nonconstant tethers and downhill walking) compared with the mean trend of 10 participants from our study. (B) Studies with exoskeletons and prostheses compared with our study. Reductions in metabolic rate compared with a Zero Force or no assistance condition versus net aiding work rate. The black line represents the effect of magnitude of conditions from the present study within 6% of the optimum peak timing (Fig. 2C). Colored lines represent trends from actuation magnitude parameter sweeps (4, 5, 7, 10–14, 16). Circles represent results from studies that do not use actuation magnitude sweep protocols (6, 9, 15, 21, 22).

in metabolic cost in individuals poststroke but no reduction using constant forces. Thus, timing could potentially have a greater influence in populations with nonconstant walking velocity, such as individuals poststroke, but this remains to be tested. Evaluating the effect of timed assistance at the COM in clinical populations requires an investigation of the targeted clinical population because there are different instances where the effects of assistive devices in healthy participants did not translate to patients (24–27). In clinical populations or older adults, it is possible that the effects of nonconstant forces on maintaining balance eliminate any metabolic cost reduction benefit. We evaluated the applicability of sinusoidal waist tether assistance in impaired gait in a healthy participant and two older adults with PAD and found that it could reduce the metabolic rate of walking. However, it is not yet possible to draw general conclusions from these small sample size experiments. Further experiments are needed to evaluate whether these results are reproducible in larger samples of patients.

Our work shows that it is possible to reduce the metabolic rate of walking by half by accelerating the COM. Although the results from our main study in healthy participants show benefits of optimally timed forces, the effects of timing were relatively small compared with the effect of aiding work rate. This could be considered as a limitation given the fact that applying different timings is more challenging than applying different constant magnitudes, which can be done with a passive tether system. Another limitation is that we only tested sinusoidal force profiles and did not evaluate whether other force profiles could provide greater assistance.

The observation that all force profiles with suboptimal timing still reduced the metabolic rate suggests that further reductions can be obtained with profiles that do not stay at a force level of 0% BW during a part of the step cycle. Using a simple pendulum model, we predict that one could approach an 80% reduction in metabolic rate by accelerating the COM during the first half of single support, followed by decelerating the COM during the second half (with a backward force) (fig. S10) (15). Such strategies could be implemented in cable robots for treadmill exercise therapy (28) or mobile devices that assist via the trunk, such as motorized rollators (29).

A number of wearable robots for clinical populations are designed to assist specifically during propulsion (30) or mimic biological kinematics or kinetics (31). We found that assisting during propulsion can reduce the metabolic rate but does not optimally reduce the metabolic rate, and even net aiding force profiles that occur entirely during braking reduce the metabolic rate. This finding indicates that bioinspired controls that mimic biological kinetics are not necessarily optimal for reducing the metabolic rate.

MATERIALS AND METHODS

Participants

Ten healthy male participants (age: 28.0 ± 4.7 years, body mass: 83.2 ± 12.2 kg, height: 1.80 ± 0.05 m, leg length: 0.993 ± 0.036 m; mean \pm SD; table S5) took part in the main study. Participants were recruited using a convenience sampling strategy. We only included participants without a previous history of musculoskeletal or neurological disorders. The sample size was selected to match the largest sample size from studies that report effects of waist tethers on metabolic rate [$n = 6$ (5), $n = 7$ (6), $n = 10$ (4, 7)] and studies with wearable robots on the effects of actuation timing and magnitude on metabolic rate [$n = 7$ (12, 32), $n = 8$ (11), $n = 9$ (21), $n = 10$ (13, 16, 33, 34)]. The researchers were not blinded to the data. The participants could

not be blinded to the conditions in which they were tested, but they were not informed about any hypothesis regarding which conditions were optimal. All participants provided written informed consent. The Institutional Review Board of the University of Nebraska Medical Center approved the study.

Protocol

The study consisted of a habituation session and a testing session 1 week later. Each session contained 1.8 hours of walking. The habituation session duration exceeded reported durations to maximize benefits from different wearable robots [40 min for a hip exosuit (35) and 105 min for an ankle exoskeleton (36)]. The testing session started with a 5-min standing trial to measure resting metabolic rate (K5, Cosmed, Rome, Italy). To ensure accurate measurement of the resting metabolic rate, we had the participant rest for at least 15 min while we prepared the experiment, and we asked the participants to have fasted for at least 5 hours, abstain from caffeine and alcohol overnight, and abstain from vigorous physical activity for 14 hours before the data collection (37). Both sessions had a 10-min warm-up, during which we cycled through all conditions and tuned the robotic tether gains. The desired treadmill speed was set to 1.25 m s^{-1} (Bertec). Near the end of the warm-up, we determined each participant's preferred step frequency under the Zero Force condition. This step frequency was used to pace the participant via a metronome to avoid walking pace changes that would affect the metabolic rate (38). Participants were able to keep their mean step time within 0.011 ± 0.008 s (mean \pm interparticipant SD from all conditions) of their instructed step time (0.562 ± 0.021 s).

Participants walked under 36 different force profiles that were randomized and grouped into three blocks, each separated by 10 min of rest (fig. S12A). Thirty-two Sinusoidal Force conditions were combinations of three desired durations (33, 66, and 99% of step time), four desired onset timings (0, 25, 50, and 75%), and different desired peak net aiding force magnitudes (ranging from 4 to 24% of BW; all force levels are reported as net aiding forces, and the tether forces were 5% higher to offset the parallel gravity component from the treadmill inclination). As with other devices (39, 40), our system had a specific bandwidth limit [3 dB bandwidth = 10 Hz (17)]. This required us to use lower peak force ranges at shorter durations (fig. S12B). We tested three conditions where the desired net aiding force remained at a constant level (4, 8, and 12% BW) throughout the step cycle (Constant Force conditions). The second-highest constant force level was chosen on the basis of the mean of the optima of earlier studies [7% (7) and 9% (4)]. We compared the effects of all the Sinusoidal and Constant Force conditions with a baseline condition where the desired net aiding force was set to 0% BW (Zero Force condition). Because of potential metabolic drift (41–43), we repeated the Zero Force condition, similar to other studies (12, 22). We also repeated one Sinusoidal Force condition that was randomly selected for each participant in each block, resulting in a total of 40 conditions. The first and last conditions of each block lasted 5 min to ensure that the metabolic rate could reach steady state. We switched between the other conditions every 2 min, and we used estimation methods from the literature (10, 44) to calculate the steady-state metabolic rate.

Measurements and data processing

Metabolic rate

Oxygen consumption and carbon dioxide production were measured using indirect calorimetry (K5, Cosmed, Rome, Italy) during the

entire protocol. We calibrated the indirect calorimetry system before every session using a gas container with a known oxygen and carbon dioxide concentration and a 3-liter fixed-volume calibration syringe that delivers simulated breath volume. The experiments occurred in a large and well-ventilated room. Breath-by-breath measurements were converted to $W\text{ kg}^{-1}$ using the Brockway equation (45). The respiratory exchange ratios were significantly lower than 1 (0.768 ± 0.053 , mean \pm interparticipant SD of all conditions, $P < 0.001$, one-sample t tests), which confirmed that the intensity level was within the aerobic range where it is appropriate to use the Brockway equation (46). We estimated the steady-state metabolic rate of the resting trial and the conditions at the beginning of each block by averaging the breath-by-breath data in the final 2 min. For all other conditions, the steady-state metabolic rates were estimated by fitting the breath-by-breath data from immediately after the transition to each new condition until right before the change to the next condition with an exponential function and estimating the asymptote (fig. S13A) (10, 44).

For each participant, we identified the time constant that minimized the squared error of the exponential fits versus the breath-by-breath metabolic rate measurements following guidelines from Selinger and Donelan (44). On the basis of the properties of our data (breath frequency of 19.8 ± 2.04 breaths min^{-1} , inter-breath SD of 0.656 ± 0.189 $W\text{ kg}^{-1}$, average change between conditions of 0.664 ± 0.193 $W\text{ kg}^{-1}$), the recommended minimum number of conditions to approximate time constants with a confidence interval of 95% is 49. Data from both sessions (80 conditions) were used to meet this recommendation for time constant identification, and the resulting time constants of our participants (46.1 ± 15.7 s, mean \pm interparticipant SD) were close to the time constants reported by Selinger and Donelan (44) (41.8 ± 12.1 s). To evaluate the metabolic rate estimation accuracy, we compared estimations based on 2 min of data with estimations that used 5 min from the final conditions of each block. The mean absolute error was $4.24 \pm 2.60\%$ of the Zero Force condition, and this result is on the lower end of a range of errors in similar methods [from 4.3% (10) up to 12.4% (47)].

We calculated the net metabolic rate by subtracting the resting metabolic rate. To evaluate metabolic drift due to the long protocol, we fit a linear trend through the net metabolic rate of the Zero Force conditions over time (fig. S13, B and C). We chose a linear fit because, according to the literature, the metabolic drift trends look predominantly linear (42, 43). The average slope of this trend during the testing session was significantly higher than zero ($P = 0.0256$, one-sample t test). Studies show that prolonged downhill running can evoke a linear drift in oxygen consumption (42, 43). Thus, the fact that walking with net aiding forces is mechanically similar to downhill locomotion might explain why a drift occurred in our experiment. To correct for the metabolic drift, we calculated all $W\text{ kg}^{-1}$ reductions in metabolic rate from the testing session versus the linear drift trend. To avoid the metabolic drift affecting normalization of the percentage reduction in metabolic rate, we divided the drift-adjusted reductions by the intercept value of the linear fit, which represented the Zero Force metabolic rate before fatigue. Analysis of the repeated Sinusoidal Force conditions showed that the drift correction improved the intraclass correlation of the repeated conditions from 0.629 to 0.766. This is considered good to excellent for intraclass correlation and is of a similar order of magnitude as reported intraclass correlations for within-session repeatability of $\dot{V}O_2$ measurements [0.87 (48)].

GRFs and COM mechanics

We measured the GRF and load cell data during the last minute of each condition. Crossover steps between belts were removed, and ~ 50 steps per condition per participant were used. The force treadmill (Bertec) was calibrated using an instrumented pole (C-motion, Germantown, MD) (49) with an accuracy threshold of ± 5 mm for the center of pressure. We minimized signal drift by zeroing between walking blocks and subtracting the median of the swing phases. The GRF and load cell (Futek) signals were smoothed with a 10-Hz low-pass filter. We chose the cutoff based on the typical frequency content of walking [6 Hz (50)] and the robotic tether bandwidth [10 Hz (17)]. We calculated the parallel and perpendicular GRFs by performing a coordinate transformation over the treadmill inclination. This inclination was verified using a bubble level and a motion capture system (VICON Vero), which was calibrated to an accuracy of 0.6 mm. There was a strong linear relationship between the mean parallel GRF and net aiding force with a slope coefficient of -1.004 ± 0.005 (mean \pm interparticipant SD), which confirmed that the calibration of both devices was consistent. To further minimize errors due to the load cell offset, we subtracted the mean sum of the parallel components of the GRF, gravity, and the load cell force based on the fact that the sum of all forces must be in equilibrium, on average.

We calculated the COM acceleration from the GRF, tether force, and gravity using Newton's second law (51). The total mass was measured by the force treadmill (Bertec), and we verified that this value corresponded to the body mass plus the added mass (~ 4.9 kg for the waist belt, calorimetry unit, shoes, and other small equipment). We calculated the velocity and position of the COM by integrating the COM acceleration (52). To obtain the COM velocity relative to a coordinate system that moves with the treadmill belt, we added the treadmill velocity. The actual treadmill velocity (1.26 m s^{-1}) was obtained by recording motion capture markers attached to the treadmill belt (53). To calculate the net aiding power, we multiplied the net aiding force by the COM velocity in the direction of the force and relative to the treadmill belt coordinate system. We calculated individual leg COM power by taking the dot product of the COM velocity and the individual (right) GRF (54). GRF recordings in 3 of the 400 trials from the testing session failed due to equipment malfunctions. For these trials, we calculated the net aiding power by assuming that the parallel COM velocity was equal to the treadmill velocity. The GRF variables of these trials were treated as missing values.

Data organization

We segmented each time series into steps and strides based on heel strike detection using the vertical GRF. For each participant and condition, we calculated the median of the strides (data S3). For the Repeated Sinusoidal Force conditions and the Zero Force condition, we averaged three repetitions of these conditions. The metabolic rate and kinetic time series were normalized relative to body mass. The peak values, step averages, and averages of positive and negative portions of tether and GRF variables were calculated from the time-normalized data (table S6). We also calculated the net aiding force duration and net aiding power duration by evaluating the length of the net aiding force and net aiding power profile that was higher than 1% BW or 0.15 W kg^{-1} . When calculating the peak force timing and peak power timing, we avoided creating artifacts in interparticipant variability from step segmentation by converting peak timings that were close to 0 or 100% to a percentage below 0% or above 100% in cases where most of the peak timings in the same

condition occurred at the opposite end of the step. For example, if the peak timing of a certain condition was 99% of the step in one participant and 1% in all the other participants, then the peak timing of 99% was converted to a value of -1%, which has the same meaning as a peak timing of 99%.

Statistical analyses

To determine the effects of the actuation profile shape parameters on the dependent parameters, we used mixed-effects model analyses with participants as random factors (21, 55, 56). To avoid overfitting, terms that did not significantly contribute were removed using a stepwise elimination procedure whereby the least significant terms were removed until only significant terms remained (57–59). Because earlier research shows that the metabolic rate follows a U-shaped trend versus aiding force magnitude (4, 7), we included first- and second-order terms for the actuation magnitude parameter. There are no prior data on the effect of actuation duration, and in light of this, we began using both first- and second-order terms for this parameter. Because the timing was varied over the entire step, we expected a continuous trend between the end of the step cycle and the beginning of the step cycle. In other words, even if the step cycle were defined differently (e.g., from toe-off to toe-off instead of from heel strike to heel strike), we would expect to see a similar (but shifted) continuous trend. Therefore, a periodic term was included for timing. We identified the mean phase shift that minimized the sum of squared errors between the model and the measurements for each participant. There cannot be an effect of duration or timing when the peak magnitude is zero, so the duration and timing terms were multiplied by the peak magnitude (13, 58). Because the actuation magnitude and reduction in metabolic rate were zero in the Zero Force condition, we did not include an intercept. Last, because we aimed to compare our results with those of devices that provide joint work and because mechanical work is a component of muscle energetic cost (60), we initially chose to express all parameters based on work rate and power instead of the average force and peak force, resulting in the following initial statistical model:

$$c_1 \cdot \dot{W}_{\text{aid}} + c_2 \cdot \dot{W}_{\text{aid}}^2 + c_3 \cdot P_{\text{peak}} \cdot \Delta t_P + c_4 \cdot P_{\text{peak}} \cdot \Delta t_P^2 + c_5 \cdot P_{\text{peak}} \cdot \sin\left(\frac{t_{P_{\text{peak}}} + c_6}{100} \cdot 2\pi\right) \quad (1)$$

where \dot{W}_{aid} is the net aiding work rate obtained by averaging the net aiding power over the step duration, P_{peak} is the peak net aiding power, Δt_P is the duration of the power burst, and $t_{P_{\text{peak}}}$ is the timing of the peak power. The metabolic rate, \dot{W}_{aid} , and P_{peak} are in W kg^{-1} . Δt_P and $t_{P_{\text{peak}}}$ are expressed in % of step time.

To evaluate these choices, we compared the estimated and actual condition averages for several alternative models (15). Because we eliminated nonsignificant terms, all terms in the final equations were significant ($P < 0.05$). We used the adjusted R^2 values to assess the added value of different numbers of predictors. The final equation after the selection of the predictors and the backward elimination of nonsignificant terms was

$$-3.13 \cdot \dot{W}_{\text{aid}} + 1.67 \cdot \dot{W}_{\text{aid}}^2 + 0.09 \cdot P_{\text{peak}} \cdot \sin\left(\frac{t_{P_{\text{peak}}} + 60.16}{100} \cdot 2\pi\right) \quad \text{Adjusted } R^2: 95.3\%$$

To analyze the Constant Force conditions, we used a model that included only the net aiding work rate terms:

$$c_1 \cdot \dot{W}_{\text{aid}} + c_2 \cdot \dot{W}_{\text{aid}}^2 \quad (2)$$

The final equation was

$$-3.25 \cdot \dot{W}_{\text{aid}} + 1.76 \cdot \dot{W}_{\text{aid}}^2 \quad \text{Adjusted } R^2: 99.8\%$$

The controller did not keep the aiding work rate constant between conditions with different timings because this would have required real-time COM velocity measurement. However, the used statistical method of linear mixed-effects model analysis does not require varying the different independent parameters in isolation [e.g., unlike approaches such as repeated-measures analysis of variance (ANOVA)]. To determine the effects of timing isolated from work, we evaluated the mixed-effects model analysis equation over the range of timings while keeping the magnitude parameters (\dot{W}_{aid} and P_{peak}) constant. To determine the effects of the net aiding work rate, we evaluated the equation while keeping the timing term that contains $t_{P_{\text{peak}}}$ constant. All statistical analyses were performed in MATLAB (MathWorks, Natick, MA, USA) using a significance threshold of 0.05. To analyze the interparticipant variability, we fit the significant terms of the equation to each participant's data using the `fminsearch` function in MATLAB, and we determined the metabolic rate, peak timing, and net aiding work rate at the optimum of each participant. This interpolated optimum was defined as the Optimum timing and magnitude, and the condition with the best mean reduction in metabolic rate was defined as the Best timing and magnitude. To evaluate differences in the metabolic rate, propulsion GRF, COM velocity, and COM power between conditions, paired t tests with Holm-Šidák correction were used for multiple comparisons (61). For statistical tests that relied on the normality assumption, we verified that the data followed a normal distribution using the Jarque-Bera test (table S6).

SUPPLEMENTARY MATERIALS

www.science.org/doi/10.1126/scirobotics.abh1925

Supplementary Materials and Methods

Supplementary Discussion

Figs. S1 to S13

Tables S1 to S6

Movie S1

Data S1 to S3

References (63–131)

REFERENCES AND NOTES

- B. R. Duffy, Anthropomorphism and the social robot. *Rob. Auton. Syst.* **42**, 177–190 (2003).
- A. J. Young, D. P. Ferris, State of the art and future directions for lower limb robotic exoskeletons. *IEEE Trans. Neural Syst. Rehabil. Eng.* **25**, 171–182 (2017).
- A. D. Kuo, Energetics of actively powered locomotion using the simplest walking model. *J. Biomech. Eng.* **124**, 113–120 (2002).
- J. S. Gottschall, R. Kram, Energy cost and muscular activity required for propulsion during walking. *J. Appl. Physiol.* **94**, 1766–1772 (2003).
- S. G. Bhat, S. Cherangara, J. Olson, S. Redkar, T. G. Sugar, Analysis of a periodic force applied to the trunk to assist walking gait. *2019 Wearable Robot. Assoc. Conf. WearRAcon 2019*, 68–73 (2019).
- K. Penke, K. Scott, Y. Sinskey, M. D. Lewek, Propulsive forces applied to the body's center of mass affect metabolic energetics poststroke. *Arch. Phys. Med. Rehabil.* **100**, 1068–1075 (2019).
- C. A. Zirker, B. C. Bennett, M. F. Abel, Changes in kinematics, metabolic cost, and external work during walking with a forward assistive force. *J. Appl. Biomech.* **29**, 481–489 (2013).
- J. Rose, J. G. Gamble, A. Burgos, J. Medeiros, W. L. Haskell, Energy expenditure index of walking for normal children and for children with cerebral palsy. *Dev. Med. Child Neurol.* **32**, 333–340 (1990).

9. J. Lee, K. Seo, B. Lim, J. Jang, K. Kim, H. Choi, Effects of assistance timing on metabolic cost, assistance power, and gait parameters for a hip-type exoskeleton. *IEEE Int. Conf. Rehabil. Robot.*, 498–504 (2017).
10. J. Zhang, P. Fiers, K. A. Witte, R. W. Jackson, K. L. Poggensee, C. G. Atkeson, S. H. Collins, Human-in-the-loop optimization of exoskeleton assistance during walking. *Science* **356**, 1280–1284 (2017).
11. R. W. Jackson, S. H. Collins, An experimental comparison of the relative benefits of work and torque assistance in ankle exoskeletons. *J. Appl. Physiol.* **119**, 541–557 (2015).
12. B. T. Quinlivan, S. Lee, P. Malcolm, D. M. Rossi, M. Grimmer, C. Sivi, N. Karavas, D. Wagner, A. Asbeck, I. Galiana, C. J. Walsh, D. Wagner, C. Sivi, M. Grimmer, S. Lee, B. T. Quinlivan, P. Malcolm, C. J. Walsh, D. M. Rossi, Assistance magnitude versus metabolic cost reductions for a tethered multiarticular soft exosuit. *Sci. Robot.* **2**, eaah4416 (2017).
13. S. Galle, P. Malcolm, S. H. Collins, D. De Clercq, Reducing the metabolic cost of walking with an ankle exoskeleton: Interaction between actuation timing and power. *J. Neuroeng. Rehabil.* **14**, 1–16 (2017).
14. I. Kang, H. Hsu, A. Young, The effect of hip assistance levels on human energetic cost using robotic hip exoskeletons. *IEEE Robot. Autom. Lett.* **4**, 430–437 (2019).
15. Supplementary Materials and Methods, Supplementary Discussion, Figures, Tables, Movie, and Data are available as supplementary materials.
16. J. M. Caputo, S. H. Collins, Prosthetic ankle push-off work reduces metabolic rate but not collision work in non-amputee walking. *Sci. Rep.* **4**, 7213 (2014).
17. A. M. Gonabadi, P. Antonellis, P. Malcolm, A system for simple robotic walking assistance with linear impulses at the center of mass. *IEEE Trans. Neural Syst. Rehabil. Eng.* **28**, 1353–1362 (2020).
18. G. A. Cavagna, F. P. Saibene, R. Margaria, External work in walking. *J. Appl. Physiol.* **18**, 1–9 (1963).
19. R. Margaria, Positive and negative work performances and their efficiencies in human locomotion. *Int. Z. Angew. Physiol.* **25**, 339–351 (1968).
20. L. C. Hunter, E. C. Hendrix, J. C. Dean, The cost of walking downhill: Is the preferred gait energetically optimal? *J. Biomech.* **43**, 1910–1915 (2010).
21. S. H. Collins, M. B. Wiggin, G. S. Sawicki, Reducing the energy cost of human walking using an unpowered exoskeleton. *Nature* **522**, 212–215 (2015).
22. L. M. Mooney, E. J. Rouse, H. M. Herr, Autonomous exoskeleton reduces metabolic cost of human walking. *J. Neuroeng. Rehabil.* **11**, 151 (2014).
23. T. G. Hornby, D. S. Reisman, I. G. Ward, P. L. Scheets, A. Miller, D. Haddad, E. J. Fox, N. E. Fritz, K. Hawkins, C. E. Henderson, K. L. Hendron, C. L. Holleran, J. E. Lysney, A. Walter, Clinical practice guideline to improve locomotor function following chronic stroke, incomplete spinal cord injury, and brain injury. *J. Neurol. Phys. Ther.* **44**, 49–100 (2020).
24. A. D. Segal, K. E. Zelik, G. K. Klute, D. C. Morgenroth, M. E. Hahn, M. S. Orendurff, P. G. Adamczyk, S. H. Collins, A. D. Kuo, J. M. Czerniecki, The effects of a controlled energy storage and return prototype prosthetic foot on transibial amputee ambulation. *Hum. Mov. Sci.* **31**, 918–931 (2012).
25. R. E. Quesada, J. M. Caputo, S. H. Collins, Increasing ankle push-off work with a powered prosthesis does not necessarily reduce metabolic rate for transibial amputees. *J. Biomech.* **49**, 3452–3459 (2016).
26. J. A. Norris, K. P. Granata, M. R. Mitros, E. M. Byrne, A. P. Marsh, Effect of augmented plantarflexion power on preferred walking speed and economy in young and older adults. *Gait Posture* **25**, 620–627 (2007).
27. Y. L. Kerkum, A. I. Buizer, J. C. Van Den Noord, J. G. Becher, J. Harlaar, M. A. Brehm, The effects of varying ankle foot orthosis stiffness on gait in children with spastic cerebral palsy who walk with excessive knee flexion. *PLOS ONE* **10**, e0142878 (2015).
28. V. Vashista, X. Jin, S. K. Agrawal, Active tethered pelvic assist device (a-tpad) to study force adaptation in human walking. *Proc. IEEE Int. Conf. Robot. Autom.*, 718–723 (2014).
29. K. H. Seo, J. J. Lee, The development of two mobile gait rehabilitation systems. *IEEE Trans. Neural Syst. Rehabil. Eng.* **17**, 156–166 (2009).
30. K. Z. Takahashi, M. D. Lewek, G. S. Sawicki, A neuromechanics-based powered ankle exoskeleton to assist walking post-stroke: A feasibility study. *J. Neuroeng. Rehabil.* **12**, 1–13 (2015).
31. G. M. Gasparri, J. Luque, Z. F. Lemer, Proportional joint-moment control for instantaneously adaptive ankle exoskeleton assistance. *IEEE Trans. Neural Syst. Rehabil. Eng.* **27**, 751–759 (2019).
32. P. Malcolm, D. M. Rossi, C. Sivi, S. Lee, B. T. Quinlivan, M. Grimmer, C. J. Walsh, Continuous sweep versus discrete step protocols for studying effects of wearable robot assistance magnitude. *J. Neuroeng. Rehabil.* **14**, 72 (2017).
33. P. Malcolm, R. E. Quesada, J. M. Caputo, S. H. Collins, The influence of push-off timing in a robotic ankle-foot prosthesis on the energetics and mechanics of walking. *J. Neuroeng. Rehabil.* **12**, 21 (2015).
34. P. Malcolm, W. Derave, S. Galle, D. De Clercq, A simple exoskeleton that assists plantarflexion can reduce the metabolic cost of human walking. *PLOS ONE* **8**, e56137 (2013).
35. F. A. Panizzolo, G. M. Freisinger, N. Karavas, A. M. Eckert-Erdheim, C. Sivi, A. Long, R. A. Zifchock, M. E. LaFiandra, C. J. Walsh, Metabolic cost adaptations during training with a soft exosuit assisting the hip joint. *Sci. Rep.* **9**, 1–10 (2019).
36. M. Bruce Wiggin, thesis, North Carolina State University (2014).
37. C. Compher, D. Frankenfield, N. Keim, L. Roth-Yousey, Best practice methods to apply to measurement of resting metabolic rate in adults: A systematic review. *J. Am. Diet. Assoc.* **106**, 881–903 (2006).
38. M. Y. Zarrugh, C. W. Radcliffe, Predicting metabolic cost of level walking. *Eur. J. Appl. Physiol. Occup. Physiol.* **38**, 215–223 (1978).
39. S. N. Simha, J. D. Wong, J. C. Selinger, J. M. Donelan, A mechatronic system for studying energy optimization during walking. *IEEE Trans. Neural Syst. Rehabil. Eng.* **27**, 1416–1425 (2019).
40. G. Brown, M. M. Wu, F. C. Huang, K. E. Gordon, Movement augmentation to evaluate human control of locomotor stability. *Proc. Annu. Int. Conf. IEEE Eng. Med. Biol. Soc. EMBS*, 66–69 (2017).
41. R. A. Robergs, D. Dwyer, T. Astorino, Recommendations for improved data processing from expired gas analysis indirect calorimetry. *Sport. Med.* **40**, 95–111 (2010).
42. K. C. Westerlind, W. C. Byrnes, R. S. Mazzeo, A comparison of the oxygen drift in downhill vs. level running. *J. Appl. Physiol.* **72**, 796–800 (1992).
43. R. W. Dick, P. R. Cavanagh, An explanation of the upward drift in oxygen uptake during prolonged sub-maximal downhill running. *Med. Sci. Sports Exerc.* **19**, 310–317 (1987).
44. J. C. Selinger, J. M. Donelan, Estimating instantaneous energetic cost during non-steady-state gait. *J. Appl. Physiol.* **117**, 1406–1415 (2014).
45. J. M. Brockway, Derivation of formulae used to calculate energy expenditure in man. *Hum. Nutr. Clin. Nutr.* **41**, 463–471 (1987).
46. S. Kipp, W. C. Byrnes, R. Kram, Calculating metabolic energy expenditure across a wide range of exercise intensities: The equation matters. *Appl. Physiol. Nutr. Metab.* **43**, 639–642 (2018).
47. K. A. Witte, P. Fiers, A. L. Sheets-Singer, S. H. Collins, Improving the energy economy of human running with powered and unpowered ankle exoskeleton assistance. *Sci. Robot.* **5**, eaay9108 (2020).
48. R. Duffield, B. Dawson, H. C. Pinnington, P. Wong, Accuracy and reliability of a Cosmed K4b2 portable gas analysis system. *J. Sci. Med. Sport* **7**, 11–22 (2004).
49. S. H. Collins, P. G. Adamczyk, D. P. Ferris, A. D. Kuo, A simple method for calibrating force plates and force treadmills using an instrumented pole. *Gait Posture* **29**, 59–64 (2009).
50. D. A. Winter, *Biomechanics and Motor Control of Human Movement* (John Wiley & Sons Inc., 2009).
51. I. Newton, *Philosophiæ Naturalis Principia Mathematica* (1687).
52. G. A. Cavagna, Force platforms as ergometers. *J. Appl. Physiol.* **39**, 174–179 (1975).
53. H. Savelberg, M. Vorstenbosch, E. H. Kamman, J. G. van de Weijer, H. C. Schamhardt, Intra-stride belt-speed variation affects treadmill locomotion. *Gait Posture* **7**, 26–34 (1998).
54. J. M. Donelan, R. Kram, A. D. Kuo, Simultaneous positive and negative external mechanical work in human walking. *J. Biomech.* **35**, 117–124 (2002).
55. A. Galecki, T. Burzykowski, Linear mixed-effects model, in *Linear Mixed-Effects Models Using R* (Springer, 2013), pp. 245–273.
56. W. P. Vispoel, Book Reviews: Statistical Reasoning for the Behavioral Sciences (2nd ed.) Richard J. Shavelson Needham Heights, MA: Allyn and Bacon, 1988. viii + 744 pp. *J. Educ. Stat.* **15**, 179–183 (1990).
57. B. X. W. Liew, S. Morris, K. Netto, The effects of load carriage on joint work at different running velocities. *J. Biomech.* **49**, 3275–3280 (2016).
58. P. Antonellis, S. Galle, D. De Clercq, P. Malcolm, Altering gait variability with an ankle exoskeleton. *PLOS ONE* **13**, e0205088 (2018).
59. P. Antonellis, C. M. Frederick, A. M. Gonabadi, P. Malcolm, Modular footwear that partially offsets downhill or uphill grades minimizes the metabolic cost of human walking. *R. Soc. Open Sci.* **7**, 191527 (2020).
60. B. R. Umberger, K. G. M. Gerritsen, P. E. Martin, A model of human muscle energy expenditure. *Comput. Methods Biomech. Biomed. Engin.* **6**, 99–111 (2003).
61. S. A. Glantz, *Primer of Biostatistics* (McGraw-Hill, 2005).
62. S. J. Abram, J. C. Selinger, J. M. Donelan, Energy optimization is a major objective in the real-time control of step width in human walking. *J. Biomech.* **91**, 85–91 (2019).
63. B. B. Lloyd, R. M. Zacks, The mechanical efficiency of treadmill running against a horizontal impeding force. *J. Physiol.* **223**, 355–363 (1972).
64. Y. H. Chang, R. Kram, Metabolic cost of generating horizontal forces during human running. *J. Appl. Physiol.* **86**, 1657–1662 (1999).
65. M. Saunders, V. Inman, H. Eberhart, The major determinants in normal and pathological gait. *J. Bone Jt. Surg.* **35**, 543–558 (1953).
66. G. A. Pratt, M. M. Williamson, Series elastic actuators. *IEEE Int. Conf. Intell. Robot. Syst.* **1**, 399–406 (1995).
67. J. Zhang, S. H. Collins, The passive series stiffness that optimizes torque tracking for a lower-limb exoskeleton in human walking. *Front. Neurobot.* **11**, 1–16 (2017).
68. S. Qian, B. Zi, W. W. Shang, Q. S. Xu, A review on cable-driven parallel robots. *Chinese J. Mech. Eng. English Ed.* **31**, 66 (2018).
69. J. Zhang, C. C. Cheah, S. H. Collins, Experimental comparison of torque control methods on an ankle exoskeleton during human walking, in *2015 IEEE International Conference on Robotics and Automation (ICRA)* (IEEE, 2015), pp. 5584–5589.

70. S. Mochon, T. A. McMahon, Ballistic walking: An improved model. *Math. Biosci.* **52**, 241–260 (1980).
71. R. M. Alexander, Simple models of human movement. *Appl. Mech. Rev.* **48**, 461–470 (1995).
72. M. Garcia, A. Chatterjee, A. Ruina, M. Coleman, The simplest walking model: Stability, complexity, and scaling. *J. Biomech. Eng.* **120**, 281–288 (1998).
73. T. McGeer, Passive dynamic walking. *Int. J. Rob. Res.* **9**, 62–82 (1990).
74. M. Srinivasan, Fifteen observations on the structure of energy-minimizing gaits in many simple biped models. *J. R. Soc. Interface* **8**, 74–98 (2011).
75. S. Faraji, A. R. Wu, A. J. Ijspeert, A simple model of mechanical effects to estimate metabolic cost of human walking. *Sci. Rep.* **8**, 1–12 (2018).
76. R. M. Alexander, Optimum muscle design for oscillatory movements. *J. Theor. Biol.* **184**, 253–259 (1997).
77. K. E. Zelik, A. D. Kuo, Human walking isn't all hard work: Evidence of soft tissue contributions to energy dissipation and return. *J. Exp. Biol.* **213**, 4257–4264 (2010).
78. A. J. Greene, P. J. Sinclair, M. H. Dickson, F. Colloud, R. M. Smith, Relative shank to thigh length is associated with different mechanisms of power production during elite male ergometer rowing. *Sport. Biomech.* **8**, 302–317 (2009).
79. A. E. Minetti, C. Moia, G. S. Roi, D. Susta, G. Ferretti, Energy cost of walking and running at extreme uphill and downhill slopes. *J. Appl. Physiol.* **93**, 1039–1046 (2002).
80. L. M. Mooney, E. J. Rouse, H. M. Herr, Autonomous exoskeleton reduces metabolic cost of human walking during load carriage. *J. Neuroeng. Rehabil.* **11**, 80 (2014).
81. J. Kim, G. Lee, R. Heimgartner, D. A. Revi, N. Karavas, D. Nathanson, I. Galiana, A. Eckert-Erdheim, P. Murphy, D. Perry, N. Menard, D. K. Choe, P. Malcolm, C. J. Walsh, Reducing the metabolic rate of walking and running with a versatile, portable exosuit. *Science* **365**, 668–672 (2019).
82. R. C. Browning, J. R. Modica, R. Kram, A. Goswami, The effects of adding mass to the legs on the energetics and biomechanics of walking. *Med. Sci. Sport. Exerc.* **39**, 515–525 (2007).
83. J. B. de V. Weir, New methods for calculating metabolic rate with special reference to protein metabolism. *J. Physiol.* **109**, 1–9 (1949).
84. C. J. Wutzke, G. S. Sawicki, M. D. Lewek, The influence of a unilateral fixed ankle on metabolic and mechanical demands during walking in unimpaired young adults. *J. Biomech.* **45**, 2405–2410 (2012).
85. I. I. Pipinos, A. R. Judge, J. T. Selsby, Z. Zhu, S. A. Swanson, A. A. Nella, S. L. Dodd, The myopathy of peripheral arterial occlusive disease: Part 1. Functional and histomorphological changes and evidence for mitochondrial dysfunction. *Vasc. Endovascular Surg.* **41**, 481–489 (2008).
86. I. I. Pipinos, A. R. Judge, J. T. Selsby, Z. Zhu, S. A. Swanson, A. A. Nella, S. L. Dodd, The myopathy of peripheral arterial occlusive disease: Part 2. Oxidative stress, neuropathy, and shift in muscle fiber type. *Vasc. Endovascular Surg.* **42**, 101–112 (2008).
87. F. G. R. Fowkes, D. Rudan, I. Rudan, V. Aboyans, J. O. Denenberg, M. M. McDermott, P. E. Norman, U. K. A. Sampson, L. J. Williams, G. A. Mensah, M. H. Criqui, Comparison of global estimates of prevalence and risk factors for peripheral artery disease in 2000 and 2010: A systematic review and analysis. *Lancet* **382**, 1329–1340 (2013).
88. B. H. Goodpaster, S. W. Park, T. B. Harris, S. B. Kritchevsky, M. Nevitt, A. V. Schwartz, E. M. Simonsick, F. A. Tykavsky, M. Visser, A. B. Newman, The loss of skeletal muscle strength, mass, and quality in older adults: The health, aging and body composition study. *J. Gerontol. Ser. A Biol. Sci. Med. Sci.* **61**, 1059–1064 (2006).
89. S. Rossi, A. Colazza, M. Petrarca, E. Castelli, P. Cappa, H. I. Krebs, Feasibility study of a wearable exoskeleton for children: Is the gait altered by adding masses on lower limbs? *PLOS ONE* **8**, e73139 (2013).
90. S. Patel, B. L. Patriitti, J. Nikitczuk, B. Weinberg, U. D. Croce, C. Mavroidis, P. Bonato, Effects on normal gait of a new active knee orthosis for hemiparetic gait retraining. *Proc. Annu. Int. Conf. IEEE Eng. Med. Biol.* **2006**, 1232–1235 (2006).
91. S. M. Cain, K. E. Gordon, D. P. Ferris, Locomotor adaptation to a powered ankle-foot orthosis depends on control method. *J. Neuroeng. Rehabil.* **4**, 48 (2007).
92. D. Torricelli, J. Gonzalez-Vargas, J. F. Veneman, K. Mombaur, N. Tsagarakis, A. J. Del-Ama, A. Gil-Agudo, J. C. Moreno, J. L. Pons, Benchmarking bipedal locomotion: A unified scheme for humanoids, wearable robots, and humans. *IEEE Robot. Autom. Mag.* **22**, 103–115 (2015).
93. L. N. Awad, J. Bae, P. Kudzia, A. Long, K. Hendron, K. G. Holt, K. O'Donnell, T. D. Ellis, C. J. Walsh, Reducing circumduction and hip hiking during hemiparetic walking through targeted assistance of the paretic limb using a soft robotic exosuit. *Am. J. Phys. Med. Rehabil.* **96**, S157–S164 (2017).
94. D. R. Carrier, C. Anders, N. Schilling, The musculoskeletal system of humans is not tuned to maximize the economy of locomotion. *Proc. Natl. Acad. Sci. U.S.A.* **108**, 18631–18636 (2011).
95. A. Grabowski, C. T. Farley, R. Kram, Independent metabolic costs of supporting body weight and accelerating body mass during walking. *J. Appl. Physiol.* **98**, 579–583 (2005).
96. J. Markowitz, H. Herr, Human leg model predicts muscle forces, states, and energetics during walking. *PLOS Comput. Biol.* **12**, e1004912 (2016).
97. B. R. Umberger, Stance and swing phase costs in human walking. *J. R. Soc. Interface* **7**, 1329–1340 (2010).
98. A. M. Gonabadi, P. Antonellis, P. Malcolm, Differences between joint-space and musculoskeletal estimations of metabolic rate time profiles. *PLOS Comput. Biol.* **16**, e1008280 (2020).
99. K. M. Newell, Y. T. Liu, G. Mayer-Kress, Time scales in motor learning and development. *Psychol. Rev.* **108**, 57–82 (2001).
100. S. Galle, P. Malcolm, W. Derave, D. De Clercq, Adaptation to walking with an exoskeleton that assists ankle extension. *Gait Posture* **38**, 495–499 (2013).
101. J. R. Koller, D. A. Jacobs, D. P. Ferris, C. D. Remy, Learning to walk with an adaptive gain proportional myoelectric controller for a robotic ankle exoskeleton. *J. Neuroeng. Rehabil.* **12**, 97 (2015).
102. K. L. Poggensee, S. H. Collins, How adaptation, training, and customization contribute to benefits from exoskeleton assistance. *Sci. Robot.* **6**, eabf1078 (2021).
103. A. H. Dewolf, Y. P. Ivanenko, R. M. Mesquita, F. Lacquaniti, P. A. Willems, Neuromechanical adjustments when walking with an aiding or hindering horizontal force. *Eur. J. Appl. Physiol.* **120**, 91–106 (2020).
104. A. J. Young, J. Foss, H. Gannon, D. P. Ferris, Influence of power delivery timing on the energetics and biomechanics of humans wearing a hip exoskeleton. *Front. Bioeng. Biotechnol.* **5**, 1–11 (2017).
105. Y. Ding, F. A. Panizzolo, C. Sivi, P. Malcolm, I. Galiana, K. G. Holt, C. J. Walsh, Effect of timing of hip extension assistance during loaded walking with a soft exosuit. *J. Neuroeng. Rehabil.* **13**, 87 (2016).
106. P. Antonellis, A. M. Gonabadi, P. Malcolm, Effects of timing and magnitude of forward forces at the waist on the metabolic cost of walking. *Am. Soc. Biomech.*, (2019).
107. R. T. Schroeder, J. L. Croft, J. E. A. Bertram, Evaluating the energetics of entrainment in a human-machine coupled oscillator system. *Sci. Rep.* **11**, 15804 (2021).
108. A. M. Jones, J. H. Doust, A 1% treadmill grade most accurately reflects the energetic cost of outdoor running. *J. Sports Sci.* **14**, 321–327 (1996).
109. K. E. Bijker, G. De Groot, A. P. Hollander, Delta efficiencies of running and cycling. *Med. Sci. Sports Exerc.* **33**, 1546–1551 (2001).
110. H.-M. Maus, S. W. Lipfert, M. Gross, J. Rummel, A. Seyfarth, Upright human gait did not provide a major mechanical challenge for our ancestors. *Nat. Commun.* **1**, 70 (2010).
111. J. Doke, Mechanics and energetics of swinging the human leg. *J. Exp. Biol.* **208**, 439–445 (2005).
112. S. H. Collins, P. G. Adamczyk, A. D. Kuo, Dynamic arm swinging in human walking. *Proc. R. Soc. B Biol. Sci.* **276**, 3679–3688 (2009).
113. J. M. Donelan, D. W. Shipman, R. Kram, A. D. Kuo, Mechanical and metabolic requirements for active lateral stabilization in human walking. *J. Biomech.* **37**, 827–835 (2004).
114. G. M. Bryan, P. W. Manks, S. C. Klein, R. J. Peuchen, S. H. Collins, A hip-knee-ankle exoskeleton emulator for studying gait assistance. *Int. J. Rob. Res.* **40**, 722–746 (2021).
115. D. Vega, C. J. Arellano, Using a simple rope-pulley system that mechanically couples the arms, legs, and treadmill reduces the metabolic cost of walking. *J. Neuroeng. Rehabil.* **18**, 96 (2021).
116. S. A. Graham, C. P. Hurt, D. A. Brown, Minimizing postural demands of walking while still emphasizing locomotor force generation for nonimpaired individuals. *IEEE Trans. Neural Syst. Rehabil. Eng.* **26**, 1003–1010 (2018).
117. C. A. Camillo, C. R. Osadnik, C. Burtin, S. Everaerts, M. Hornikx, H. Demeyer, M. Loeckx, F. M. Rodrigues, K. Maes, G. Gayan-Ramirez, W. Janssens, T. Troosters, Effects of downhill walking in pulmonary rehabilitation for patients with COPD: A randomised controlled trial. *Eur. Respir. J.* **56**, 2000639 (2020).
118. S. Carda, M. Invernizzi, A. Baricich, G. Cognolato, C. Cisari, Does altering inclination alter effectiveness of treadmill training for gait impairment after stroke? A randomized controlled trial. *Clin. Rehabil.* **27**, 932–938 (2013).
119. Sloan M. Zimmerman, thesis, The Ohio State University (2016).
120. J. Kerestes, T. G. Sugar, Enhanced running using a jet pack. *Proc. ASME 2014 Int. Des. Eng. Tech. Conf. Comput. Inf. Eng. Conf.*, 1–7 (2014).
121. M. Finn-Henry, A. Baimyshev, M. Goldfarb, Feasibility study of a fall prevention cold gas thruster, in *Proceedings of the IEEE RAS and EMBS International Conference on Biomedical Robotics and Biomechanics* (IEEE, 2020), pp. 611–616.
122. W. C. Miller, M. Speechley, B. Deathe, The prevalence and risk factors of falling and fear of falling among lower extremity amputees. *Arch. Phys. Med. Rehabil.* **82**, 1031–1037 (2001).
123. K. C. Bairapareddy, P. Jirange, K. Vaishali, Gait parameters, balance and risk of falls in COPD: Cross sectional study, in *9.2 Physiotherapists* (European Respiratory Society, 2016), p. OA4820.
124. M. F. Reelick, M. B. van Iersel, R. P. C. Kessels, M. G. M. Olde Rikkert, The influence of fear of falling on gait and balance in older people. *Age Ageing* **38**, 435–440 (2009).
125. A. Schinkel-Ivy, E. L. Inness, A. Mansfield, Relationships between fear of falling, balance confidence, and control of balance, gait, and reactive stepping in individuals with sub-acute stroke. *Gait Posture* **43**, 154–159 (2016).

126. T. G. Sugar, A. Bates, M. Holgate, J. Kerestes, M. Mignolet, P. New, R. K. Ramachandran, S. Redkar, C. Wheeler, Limit cycles to enhance human performance based on phase oscillators. *J. Mech. Robot.* **7**, 011001 (2015).
127. R. Matsuzaki, Y. Fujimoto, Walking assist device using Control Moment Gyroscopes, in *IECON Proceedings (Industrial Electronics Conference)* (IEEE, 2013), pp. 6581–6586.
128. D. Li, H. Vallery, Gyroscopic assistance for human balance, in *International Workshop on Advanced Motion Control, AMC* (IEEE, 2012), pp. 1–6.
129. S. Jabeen, A. Berry, T. Geijtenbeek, J. Harlaar, H. Vallery, Assisting gait with free moments or joint moments on the swing leg. *IEEE Int. Conf. Rehabil. Robot.* **2019**, 1079–1084 (2019).
130. T. L. Brown, J. P. Schmiedeler, Reaction wheel actuation for improving planar biped walking efficiency. *IEEE Trans. Robot.* **32**, 1290–1297 (2016).
131. J. A. M. Haarman, E. Maartens, H. van der Kooij, J. H. Buurke, J. Reenalda, J. S. Rietman, Manual physical balance assistance of therapists during gait training of stroke survivors: Characteristics and predicting the timing. *J. Neuroeng. Rehabil.* **14**, 125 (2017).

Acknowledgments: We would like to thank A. Harp, M. Fritton, and A. Dzewaltowski for assistance with pilot testing and data processing; A. Skiadopoulos for assistance with calibrations and additional analyses; and B. Senderling, T. Vanderheyden, and HuMoTech for technical support. We would also like to thank G. Lee, J. Kim, J. Caputo, K. Takahashi, N. Hunt, M. Donelan, and the members of the SFU Locomotion Laboratory for suggestions for improving the manuscript and R. Kram for thoughtful conversations on the experiments.

Funding: This work was supported by the Center for Research in Human Movement Variability of the University of Nebraska at Omaha, NIH grant number P20GM109090 to P.M., Nebraska EPSCOR First grant number OIA-1557417 to P.M., and a Graduate Research and Creative Activity (GRACA) grant from the University of Nebraska at Omaha and an AMTI Force and Motion Foundation award to P.A. This work received additional support from NIH grant numbers R01HD090333 to S.A.M. and R01AG034995 and R01AG049868 to I.I.P. and U.S. Department of Veterans Affairs Rehabilitation Research and Development Service grant number I01RX003266 to S.A.M. **Author contributions:** P.A. and P.M. conceived the study concept and experimental methods. A.M.G. conceived and implemented the control and pulley hardware. P.A. and A.M.G. conducted the main experiments. P.A., A.M.G., S.A.M., and I.I.P. conducted the supplementary analyses. A.M.G. and P.M. conducted the simple pendulum model analyses. P.A. and A.M.G. processed the data. P.A. and P.M. prepared the manuscript. All authors revised and approved the final manuscript. **Competing interests:** S.A.M. serves on the advisory board and as a consultant for DigiTrans LLC. The other authors declare that they have no competing interests. **Data and materials availability:** All data needed to support the conclusions of this manuscript are included in the main text or Supplementary Materials. Source data are available in the Supplementary Materials.

Submitted 22 February 2021
Accepted 18 February 2022
Published 16 March 2022
10.1126/scirobotics.abh1925

Metabolically efficient walking assistance using optimized timed forces at the waist

Prokopios Antonellis, Arash Mohammadzadeh Gonabadi, Sara A. Myers, Iraklis I. Pipinos, and Philippe Malcolm

Sci. Robot. **7** (64), eabh1925. DOI: 10.1126/scirobotics.abh1925

View the article online

<https://www.science.org/doi/10.1126/scirobotics.abh1925>

Permissions

<https://www.science.org/help/reprints-and-permissions>

Use of this article is subject to the [Terms of service](#)

Science Robotics (ISSN 2470-9476) is published by the American Association for the Advancement of Science, 1200 New York Avenue NW, Washington, DC 20005. The title *Science Robotics* is a registered trademark of AAAS.

Copyright © 2022 The Authors, some rights reserved; exclusive licensee American Association for the Advancement of Science. No claim to original U.S. Government Works